

*Supplementary Information*

**Revealing uncommon transport in the previously unascertained very low cation clathrate-I  $\text{Eu}_2\text{Ga}_{11}\text{Sn}_{35}$**

Wilarachchige D. C. B. Gunatilleke,<sup>a</sup> Winnie Wong-Ng,<sup>b</sup> Peter Y. Zavalij,<sup>c</sup> Mingjian Zhang,<sup>d</sup> Yu-Sheng Chen,<sup>d</sup> and  
George S. Nolas<sup>\*a</sup>

<sup>a</sup> Department of Physics, University of South Florida, Tampa, FL 33620, USA

<sup>b</sup> Materials Measurement Science Division, National Institute of Standards and Technology, Gaithersburg, MD  
20899, USA

<sup>c</sup> Department of Chemistry and Biochemistry, University of Maryland, College Park, MD 20742, USA

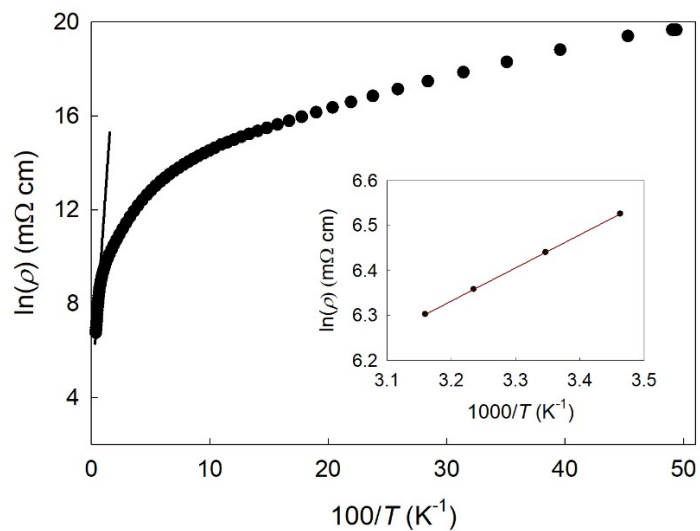
<sup>d</sup> ChemMatCARS, University of Chicago, Argonne, IL 60439, USA

Resistivity and Seebeck Coefficient measurements employing the transport option of the Physical Property Measurements System (PPMS) from Quantum Design were performed using two voltage leads and two current or temperature leads for resistivity and Seebeck Coefficient, respectively, in a two-probe configuration. The leads, Au coated manganin, were attached to the specimen using silver epoxy (H20E). The single crystal used for the measurements was approximately  $1.25 \times 1.25 \times 1.25 \text{ mm}^3$  as estimated by measurements of the dimensions of the facets. Figure S1 shows temperature dependent resistivity,  $\rho$ , data used to obtain a band gap,  $E_g$ , of 0.13 eV. Temperature dependent Hall coefficient was measured using the resistivity option of PPMS at 3 different maximum magnetic fields of 1.2 T, 2.4 T and 4.8 T. A measurement sequence was set up to allow the field to alternate direction at each field.

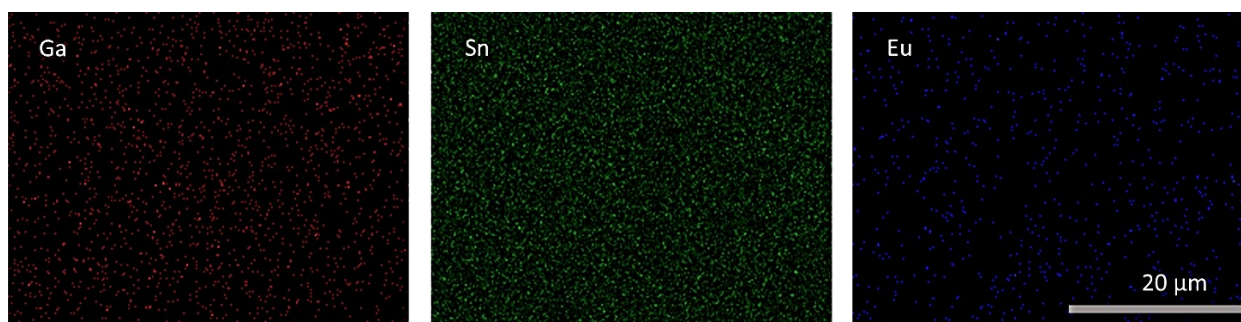
$\text{Eu}_2\text{Ga}_{11}\text{Sn}_{35}$  forms in the cubic clathrate-I (space group  $Pm\bar{3}n$ , No. 223) structure with a lattice parameter  $a$  of 11.9497(5) Å at 298 K. Dodecahedra  $(\text{Sn}/\text{Ga})_{20}$  and tetrakaidekahedra  $(\text{Sn}/\text{Ga})_{24}$  can be thought of as forming the framework such that Eu reside at the center of the two polyhedra formed by the framework at the  $2a$  and  $6d$  sites, respectively. Unlike typical clathrate-I compositions, Eu partially occupies both sites with no split-position detected while 24 % of the framework has Ga substituting for Sn in all three framework sites with a preferential occupancy at the  $6c$  site, as is typical of other clathrate-I compositions<sup>1-5</sup>. The structural refinements yielded the composition  $\text{Eu}_{2.2(2)}\text{Ge}_{11.0(2)}\text{Sn}_{35.0(2)}$ . The independent refinement of each of the Wyckoff positions yielded partial occupancy of  $2a$  and  $6d$  sites by Eu, and mixed occupancy at  $16i$ ,  $24k$  and  $6c$  by Ga and Sn (Table S2). The total occupation of all sites is fully correlated with the scale factor; for each of the  $16i$ ,  $24k$  and  $6c$  sites the Ga:Sn ratio was refined independently, with full occupation of the framework sites.

Table S1 and S2 provides single-crystal structure and atomic coordinates with equivalent isotropic atomic displacement parameters, respectively. Table S3 and S4 provide the anisotropic displacement parameters and bond distances, respectively. Figure 1 in the main text of the manuscript illustrates the positions of the Eu in both crystallographic sites. A JEOL JSM-6390LV Scanning Electron Microscope (SEM) equipped with an Oxford INCA X-Sight 7852 for Energy Dispersive Spectroscopy (EDS) was employed to corroborate our XRD data. Figure S2 shows EDS elemental mapping images that corroborate the  $\text{Eu}_2\text{Ga}_{11}\text{Sn}_{35}$  stoichiometry as well as illustrate the homogeneity of the specimen.

As shown in Table S4, the Eu-to-framework bond distances in  $(\text{Ga}/\text{Sn})_{20}$  range from 3.7913(3) Å to 3.9882(2) Å and the guest-host distances in  $(\text{Ga}/\text{Sn})_{24}$  range from 3.9912(2) to 4.6295(3) Å. The framework bond distances are in the range of 2.7443(2) Å to 2.8115(4) Å, bond lengths that are within the range of those reported for Ga-Ga<sup>6</sup> and Sn-Sn bonds<sup>7</sup>, as well as calculated Sn-Sn bond distances for  $\text{Sn}_{46}$ <sup>8,9</sup>. The  $6c$  site preference of Ga may be partially due to its smaller size, however, topological charge stabilization<sup>10</sup> and the Mulliken population analysis<sup>11</sup> may also play a role; the electropositive (or less electronegative) species will occupy the framework sites with the lowest Mulliken population while more electronegative species will prefer the sites with the highest Mulliken population. In  $\text{Eu}_{2.2}\text{Ga}_{11}\text{As}_{35}$  the  $6c$  site has the lowest Mulliken population therefore Ga, which is less electronegative ( $\chi_{\text{Ga}} = 1.81$ ) than Sn ( $\chi_{\text{Sn}} = 1.96$ )<sup>12</sup>, would be expected to preferentially substitute on this site, as confirmed by our experimental results.



**Figure S1.**  $\ln(\rho)$  vs.  $100/T$ , where the solid line (magnified in the inset for clarity) is a fit of the form  $\rho = \rho_0 \exp(E_g/2k_B T)$  resulting in  $E_g = 0.13$  eV.



**Figure S2.** EDS elemental mapping of a surface of a representative crystal of  $\text{Eu}_2\text{Ga}_{11}\text{Sn}_{35}$ .

**Table S1.** Crystal data and structure refinement data at 298K.

Empirical formula	$\text{Eu}_{2.2(2)}\text{Ga}_{11.0(2)}\text{Sn}_{35.0(2)}$
-------------------	--

Formula weight	5258.42
Temperature/K	298 K
Crystal system, Space group	cubic, $Pm\bar{3}n$
a/Å, Volume/Å <sup>3</sup>	11.9497(5), 1706.4(7)
Z, $\rho_{\text{calc}}/\text{g cm}^{-3}$	1, 5.117
$\mu/\text{mm}^{-1}$ , F(000)	18.020, 2231
Crystal size/mm <sup>3</sup>	0.12 x 0.11 x 0.06
Radiation, 2 $\Theta$ range for data collection/°	Synchrotron ( $\lambda = 0.41328$ Å), 2.0 to 31.14
Index ranges	-15 ≤ h ≤ 15, -15 ≤ k ≤ 15, -15 ≤ l ≤ 15
Reflections collected, Independent reflections	39436, 380 [ $R_{\text{int}} = 0.0646$ , $R_{\text{sigma}} = 0.0098$ ]
Data/restraints/parameters	380/1/21
Goodness-of-fit on F <sup>2</sup> , Final R indexes [ $I \geq 4\sigma(I)$ ]	1.225, R1 = 0.0095, wR2 = 0.0216
Largest diff. peak/hole / e Å <sup>-3</sup>	0.55/-0.36

$$R_1 = \frac{\sum ||F_o| - |F_c||}{\sum |F_o|}, \quad wR_2 = \frac{[\sum w(F_o^2 - F_c^2)^2 / \sum w(F_o^2)^2]^{1/2}}{\sum w(F_o^2)^2}$$

\*  $U_{\text{eq}}$  is defined as one third of the trace of the orthogonalized  $U_{ij}$  tensor.

**Table S2.** Atomic coordinates and equivalent\* isotropic atomic displacement parameters (Å<sup>2</sup>) at 298K.  $U_{\text{eq}}$  is defined as one third of the trace of the orthogonalized  $U_{ij}$  tensor.

Atom	x/a	y/b	z/c	$U_{\text{eq}}$	Atomic occupancy	# positions
Eu1	0.0000	0.0000	0.0000	0.0365(7)	0.274(2)	2a
Eu2	0.5	0.75	0.0	0.0984(12)	0.278(3)	6d
Sn1/Ga1	0.68318(2)	0.68318(2)	0.68318(2)	0.01530(11)	0.849(3)/0.151(3)	16i
Sn2/Ga2	0.61764(2)	0.5	0.81233(2)	0.01580(10)	0.771(2)/0.229(2)	24k
Sn3/Ga3	0.75	0.5	0	0.0172(2)	0.486(6)/0.514(6)	6c

**Table S3.** Anisotropic Displacement Parameters (Å<sup>2</sup>) at 298K. The Anisotropic displacement factor exponent takes the form:  $-2\pi^2[h^2a^*U_{11} + \dots + 2hka^*b^*U_{12}]$ .

Atom	$U_{11}$	$U_{22}$	$U_{33}$	$U_{23}$	$U_{13}$	$U_{12}$
Eu1	0.0366(7)	0.0366(7)	0.0366(7)	0	0	0
Eu2	0.122(2)	0.0515(11)	0.122(2)	0	0	0
Sn1/Ga1	0.01530(11)	0.01530(11)	0.01530(11)	-0.00070(4)	-0.00070(4)	-0.00070(4)
Sn2/Ga2	0.01536(12)	0.01580(12)	0.01626(12)	0	-0.00008(6)	0
Sn3/Ga3	0.0176(2)	0.0170(2)	0.0170(2)	0	0	0

**Table S4.** Selected atomic distances (Å) and bond angles (°) at 298 K.

### Bond Lengths

Eu1-(Ga/Sn)1	3.7912(3)
-(Ga/Sn)2	3.9882(2)
Eu2-(Ga/Sn)1	4.4455(2)
-(Ga/Sn)2	4.6295(3)
-(Ga/Sn)2	3.9912(2)
-(Ga/Sn)3	4.2249(2)
(Ga/Sn)3-(Ga/Sn)2	2.7443(2)
(Ga/Sn)1-(Ga/Sn)2	2.7904(2)
(Ga/Sn)2-(Ga/Sn)2	2.8115(4)
(Ga/Sn)1-(Ga/Sn)1	2.7663(4)

### Bond Angles

(Ga,Sn)1-(Ga,Sn)1-(Ga,Sn)2	107.193(5)
(Ga,Sn)2-(Ga,Sn)1-(Ga,Sn)2	111.650(5)
(Ga,Sn)1-(Ga,Sn)2-(Ga,Sn)1	103.335(7)
(Ga,Sn)1-(Ga,Sn)2-(Ga,Sn)2	106.299(4)
(Ga,Sn)2-(Ga,Sn)2 (Ga,Sn)3	125.194(4)
(Ga,Sn)1-(Ga,Sn)2-(Ga,Sn)3	106.872(6)
(Ga,Sn)2-(Ga,Sn)3-(Ga,Sn)2	109.402(4)
(Ga,Sn)2-(Ga,Sn)3-(Ga,Sn)2	109.609(7)

---

### References

1. A. Czybulka, B. Kuhl, H. -U. Schuster, *Z. Anorg. Allg. Chem.*, 1991, **594**, 23.

2. A. P. Wilkinson, C. Lind, R. A. Young, S. D. Shastri, P. L. Lee, G. S. Nolas, *Chem. Mater.*, 2002, **14**, 1300.
3. T. Kawaguchi, K. Tanigaki, M. Yasukawa, *Appl. Phys. Lett.*, 2000, **77**, 3438.
4. Y. Zhang, P. L. Lee, G. S. Nolas, A. P. Wilkinson, *Appl. Phys. Lett.*, 2002, **80**, 2931.
5. K. Wei, A. R. Khabibullin, D. Hobbis, W. Wong-Ng, T. Chang, S. G. Wang, I. Levin, Y. S. Chen, L. M. Woods, G. S. Nolas, *Inorg. Chem.*, 2018, **57**, 9327.
6. Computational Chemistry Comparison and Benchmark DataBase, Release 19, April 2018. National Institute of Standards and Technology, US Department of Commerce.
7. K. Zeckert, *Inorganics*, 2016, **4**, 19.
8. C. W. Myles, J. Dong, O. F. Sankey, *Phys. Rev. B*, 2001, **64**, 165202.
9. A. R. Khabibullin, T. D. Huan, G. S. Nolas, L. M. Woods, *Acta Mater.*, 2017, **131**, 475.
10. B. M. Gimarc, *J. Am. Chem. Soc.*, 1983, **105**, 1979.
11. G. J. Miller, *Chemistry, Structure, and Bonding of Zintl Phases and Ions*; S.M. Kauzlarich, Eds; VCH: New York; 1996, pp 1-59.
12. Pauling, L. *The Nature of the Chemical Bond*, Cornell Univ., USA, 3rd ed., 1960.